ATLAS NOTE

ATLAS-CONF-2014-017

April 1, 2014

Search for high-mass states with one lepton plus missing transverse momentum in *pp* collisions at $\sqrt{s} = 8$ TeV with the ATLAS detector

The ATLAS Collaboration

Abstract

A search is presented for new high-mass states decaying to a lepton (electron or muon) plus missing transverse momentum using 20.3 fb^{-1} of proton-proton collision data at $\sqrt{s} = 8$ TeV recorded with the ATLAS experiment at the Large Hadron Collider. No significant excess beyond Standard Model expectations is observed. A W' with Sequential Standard Model couplings is excluded at the 95% credibility level for masses up to 3.27 TeV. Excited chiral bosons (W^*) with equivalent coupling strengths are excluded for masses up to 3.17 TeV. Limits on the mass scale M_* of the unknown mediating interaction for dark matter pair production in association with a leptonically decaying W are also set.

1 Introduction

High-energy collisions at CERN's Large Hadron Collider (LHC) provide new opportunities to search for physics beyond the Standard Model (SM) of strong and electroweak interactions. One extension common to many models is the existence of additional heavy gauge bosons, of which the charged are commonly denoted W'. Such particles are most easily searched for in their decay to a charged lepton (either electron or muon) and a neutrino.

This note describes such a search performed using 8 TeV pp collision data collected with the ATLAS detector during 2012 corresponding to a total integrated luminosity of 20.3 fb^{-1}. The data are used to extend current limits [1–6]. Limits are evaluated in the context of the Sequential Standard Model (SSM), the extended gauge model of ref. [7] with the W' coupling to WZ set to zero. In this model, the W' has the same couplings to fermions as the SM W boson and a width that increases linearly with the W' mass.

A search is also performed for the charged partners, denoted W^*, of the chiral boson excitations described in ref. [8] with theoretical motivation in ref. [9]. The anomalous (magnetic-moment type) coupling of the W^* leads to kinematic distributions significantly different from those of the W' as demonstrated in the previous ATLAS search [6] for this resonance that was performed using 7 TeV pp collision data collected in 2011 corresponding to an integrated luminosity of 4.7 fb^{-1}. The search region is expanded to higher masses and the limits are considerably improved in the region covered by the previous search. A lower mass limit is evaluated by fixing the W^* coupling strengths to give the same partial decay widths as the SSM W' .

The analysis presented here identifies event candidates in the electron and muon channels, sets separate limits for $W'/W^* \to e\nu$ and $W'/W^* \to \mu\nu$, and then combines these assuming a common branching fraction for the two final states. The kinematic variable used to identify the W'/W^* is the transverse mass

$$m_{\mathrm{T}} = \sqrt{2 p_{\mathrm{T}} E_{\mathrm{T}}^{\mathrm{miss}} (1 - \cos \varphi_{\ell\nu})}, \tag{1}$$

where p_{T} is the lepton transverse momentum, $E_{\mathrm{T}}^{\mathrm{miss}}$ is the magnitude of the missing transverse momentum vector (missing E_{T}), and $\varphi_{\ell\nu}$ is the angle between the p_{T} and missing E_{T} vectors. Here and in the following, transverse refers to the plane perpendicular to the colliding beams, longitudinal means parallel to the beams, θ and φ are the polar and azimuthal angles with respect to the longitudinal direction, and pseudorapidity is defined as $\eta = -\ln(\tan(\theta/2))$.

The signal region for this analysis (defined in more detail later) is restricted to high m_{T} which results in a large uncertainty on the signal efficiency for large W' masses. At the highest masses probed by this analysis, a significant fraction of the signal production is far off-shell, with $m_{\ell\nu} \ll m_{W'}$, where $m_{W'}$ is the pole mass of the W'. The uncertainty for the mass-dependent higher order QCD signal cross-section corrections at high mass is dominated by the parton distribution functions (PDFs) uncertainty and increases quickly for masses above about 2 TeV. The combination of these two effects results in a larger uncertainty in the signal region than for the full phase space, and therefore, a large uncertainty on the signal efficiency for large W' masses. The uncertainty on the signal selection efficiency is reduced by restricting to a phase space region with large invariant mass. In this note, limits are set on the signal cross-section times branching fraction (σB), defined as the product of total cross-section multiplied by the $W'/W^* \to \ell\nu$ branching fraction and then multiplied by the acceptance of events passing the requirement $m_{\ell\nu} > 0.4\, m_{W'/W^*}$ at the generator level. This phase space region encloses the signal region for the highest W' masses in such a way that the contribution in the signal region from events failing the requirement is marginal.

The data are also used to set limits on the production of weakly interacting candidate dark matter (DM) particles. They can be pair produced at the LHC, $pp \to \chi\bar{\chi}$, via a new intermediate state. Since DM particles do not interact with the detector material, their production leads to only an $E_{\mathrm{T}}^{\mathrm{miss}}$ signature. However, these events can be detected if there is associated initial-state radiation of a SM particle [10].

Both Tevatron and LHC collaborations have reported limits on the cross-section of $pp \to \chi\bar{\chi} + X$ where X is a hadronic jet [10–12], a photon [13, 14] or hadronically decaying W or Z boson [15]. Previous LHC results have also been reinterpreted to set limits on the scenarios where X is a leptonically decaying W [16] or Z [17, 18] boson, and this analysis is the first direct ATLAS search for the former case. Limits are reported in terms of the mass scale M_* of a new SM-DM interaction expressed in an effective field theory as a four-point contact interaction [19–27]. As discussed in the literature, e.g. refs. [28, 29], the effective field theory formalism becomes a poor approximation if the mass of the intermediate state is below the momentum transferred in the interaction, but this issue is not addressed any further in this note. Four effective operators are used as a representative set based on the definitions in ref. [23]: $D1$ scalar, $D5$ vector (both constructive and destructive interference cases, prior denoted as $D5c$ and latter $D5d$) and $D9$ tensor. In contrast to the W'/W^* limits, limits on M_* in the DM search are evaluated using the total cross-section times branching fraction σB.

The main background to the $W'/W^* \to \ell\nu$ signal comes from the high-m_T tail produced by SM W boson decays to the same final state. Other backgrounds are Z bosons decaying into two leptons where one lepton is not reconstructed, W or Z decaying to τ leptons where a τ subsequently decays to an electron or muon, and diboson production. These are collectively referred to as the electroweak (EW) background. In addition, there is a background contribution from $t\bar{t}$ and single-top production, collectively referred to as top background, which is most important for the lowest W' masses considered here, where it constitutes about 10% of the background after event selection in the electron channel and 15% in the muon channel. Other strong-interaction background sources, where a light or heavy hadron decays semileptonically or a jet is misidentified as an electron, are estimated to be at most 5% of the total background in the electron channel and a small fraction at the percent level in the muon channel. These are called QCD background in the note.

2 ATLAS Detector

The ATLAS detector [30] is a multipurpose particle detector with forward-backward symmetric cylindrical geometry covering the pseudorapidity range $|\eta| <2.5$ for measurement of charged particles and $|\eta| <4.9$ for all particles except for neutrinos. The inner tracking detector (ID) consists of a silicon pixel detector, a silicon microstrip detector, and a straw-tube transition radiation tracker. The ID is surrounded by a thin superconducting solenoid, providing a 2 T magnetic field, and then by a high-granularity liquid-argon (LAr) sampling electromagnetic (EM) calorimeter. A steel and scintillator tile calorimeter is located outside the LAr EM calorimeter and provides hadronic coverage in the central rapidity range. The end-cap and forward regions are instrumented with LAr calorimetry with copper or tungsten as the absorber for electromagnetic and hadronic measurements. The muon spectrometer (MS) surrounds the calorimeters and consists of three large superconducting toroid systems (each with eight coils) together with multiple layers of trigger and tracking chambers, providing precision track measurement for $|\eta| <2.7$ and triggering for $|\eta| <2.4$.

3 Trigger and Reconstruction

The data used in the electron channel were recorded with a trigger requiring the presence of an EM cluster (that is an energy cluster in the EM compartment of the calorimeter) with energy corresponding to an electron with $p_\mathrm{T} > 120$ GeV. For the muon channel, matching tracks in the MS and ID with combined $p_\mathrm{T} > 36$ GeV are used to select events. In order to decrease loss in selection efficiency due to the trigger, events are also recorded if a muon with $p_\mathrm{T} > 40$ GeV and $|\eta| < 1.05$ is found in the MS. The average trigger efficiency (measured with respect to reconstructed objects) is above 99% in the electron channel and 80–90% in the muon channel in the region of interest.

Each EM cluster with $E_T > 125$ GeV and $|\eta| < 1.37$ (central region) or $1.52 < |\eta| < 2.47$ (forward region) is considered as an electron candidate if it matches an inner detector track. The electron direction is defined as that of the reconstructed track and its energy as that of the cluster, with a small η-dependent energy scale correction. In the high-E_T range relevant to this analysis, the calorimeter energy resolution is measured in data to be 1.2% in the central region and 1.8% in the forward region [31]. To discriminate against hadronic jets, requirements are imposed on the lateral shower shapes in the first two layers of the EM compartment of the calorimeter and on the fraction of energy leaking into the hadronic compartment. These requirements result in about 90% identification efficiency for electrons with $E_T > 125$ GeV.

Muons are required to have $p_T > 45$ GeV, where the momentum of the muon is obtained by combining the ID and MS measurements. To ensure an accurate measurement of the momentum, muons are required to have hits in all three muon layers and are restricted to the following η-ranges approximately $|\eta| < 1.0$ and $1.3 < |\eta| < 2.0$. Including the muon candidates with η-range up to $|\eta| <2.5$ leads to signal efficiency increase up to 12% for lower W' masses, and up to 3% for W' mass of 3 TeV. However, there is a substantial increase to the background levels, over 15% in the signal region. For the final selection of good muon candidates, the individual ID and MS momentum measurements are required to be in agreement within 5 standard deviations of their errors. The average momentum resolution is about 15%–20% at $p_T = 1$ TeV. About 80% of the muons in these η-ranges are reconstructed, with most of the loss coming from regions with limited detector coverage.

The missing E_T in each event is evaluated by summing over energy-calibrated physics objects (jets, photons and leptons) and adding corrections for calorimeter deposits away from these objects [32].

This analysis makes use of all the $\sqrt{s} = 8$ TeV data collected in 2012 for which the relevant detector systems were operating properly. The integrated luminosity for the data used in this study is 20.3 fb^{-1} in both the electron and muon decay channels. The uncertainty on this measurement is 2.8%, which is derived following the methodology detailed in ref. [33].

4 Monte Carlo Simulation

With the exception of the QCD background, which is estimated from data, expected signals and backgrounds are evaluated using simulated samples, normalized with calculated cross-sections and the integrated luminosity of the data.

The W' signal events are generated at leading-order (LO) with Pythia v8.165 [34] using the MSTW-2008 LO [35] PDFs. Pythia is also used for the $W^* \to \ell\nu$ event generation, but with initial kinematics generated at LO with CalcHEP [36] using the the MSTW2008 LO PDFs. DM signal samples were produced using a Madgraph5 v1.4.5 [37] implementation interfaced to Pythia v8.165 for the parton shower and hadronization.

The W/Z boson and the $t\bar{t}$ backgrounds are generated at next-to-leading-order (NLO) with Powheg-Box r1556 [38] using the CT10 NLO [39] PDFs along with Pythia v8.165 for the fragmentation and hadronization. The single-top background is generated at NLO with MC@NLO v4.06 [40] using the CT10 NLO PDFs for the Wt and s-channels, and with AcerMC v3.8 [41] using CTEQ6L1 PDFs for the t-channel. Fragmentation and hadronization for the MC@NLO samples is performed with Herwig v6.520 [42], using Jimmy v4.31 [43] for the underlying event, whereas Pythia v6.426 is used for the AcerMC samples. The WW,WZ and ZZ diboson backgrounds are generated at multi-leg LO with Sherpa v1.4.1 [44] using the CT10 NLO PDFs.

The Pythia signal model for W' has $V-A$ SM couplings to fermions but does not include interference between W and W'. For both W' and W^*, decays to channels other than $e\nu$ and $\mu\nu$, including $\tau\nu$, ud, sc and tb, are included in the calculation of the widths but are not explicitly included as signal or background. At high mass ($m_{W'} > 1$ TeV), the branching fraction to each of the lepton decay channels is 8.2%.

For all samples, final-state photon radiation from leptons is handled by Photos [45]. The ATLAS

Table 1: Predicted values of σB for $W' \to \ell\nu$, $W^* \to \ell\nu$, and corresponding acceptances for the requirement $m_{\ell\nu} > 0.4\, m_{W'/W^*}$. The σB for $W' \to \ell\nu$ are at NNLO while those for $W^* \to \ell\nu$ are at LO. The values are exclusive and are used for both $\ell = e$ and $\ell = \mu$. The uncertainties on the acceptance for $W' \to \ell\nu$ are calculated from variations of the MSTW 2008 NNLO PDF at 90% CL, while the uncertainties arising from renormalisation and factorisation scale variations are negligible with respect to the ones for PDFs and hence neglected. For the $W^* \to \ell\nu$, PDF uncertainties on the acceptance have been neglected due to the non-renormalizability of the $W^* \to \ell\nu$ model.

Mass	$W' \to \ell\nu$		$W^* \to \ell\nu$	
[GeV]	σB [pb]	Acceptance	σB [pb]	Acceptance
300	149.0	$0.990^{+0.010}_{-0.038}$		
400	50.2	$0.988^{+0.012}_{-0.041}$	37.9	1.00
500	21.4	$0.985^{+0.015}_{-0.044}$	16.5	1.00
600	10.4	$0.983^{+0.017}_{-0.048}$	8.08	1.00
750	4.16	$0.978^{+0.022}_{-0.053}$	3.24	1.00
1000	1.16	$0.969^{+0.031}_{-0.063}$	0.904	1.00
1250	0.389	$0.956^{+0.044}_{-0.076}$	0.299	1.00
1500	0.146	$0.935^{+0.065}_{-0.090}$	0.109	1.00
1750	0.0581	$0.91^{+0.09}_{-0.11}$	0.0417	1.00
2000	0.0244	0.86 ± 0.12	0.0165	1.00
2250	0.0108	0.79 ± 0.14	0.00661	1.00
2500	0.00509	0.69 ± 0.15	0.00267	1.00
2750	0.00258	0.56 ± 0.15	0.00108	1.00
3000	0.00144	0.43 ± 0.14	4.35×10^{-4}	1.00
3250	0.000885	0.31 ± 0.11	1.75×10^{-4}	0.99
3500	0.000588	0.209 ± 0.079	7.05×10^{-5}	0.99
3750	0.000419	0.144 ± 0.054	2.85×10^{-5}	0.98
4000	0.000312	0.101 ± 0.036	1.17×10^{-5}	0.96

full detector simulation [46] based on Geant4 [47] is used to propagate the particles and account for the response of the detector. For the underlying event, the ATLAS tune AUET2B [48] is used. The effect of multiple proton-proton collisions from the same or nearby beam bunch crossings (in-time or out-of-time pile-up) is incorporated into the simulation by overlaying additional minimum-bias events generated with Pythia onto hard-scatter events. Simulated events are weighted to match the distribution of the number

Table 2: Predicted values of σB for DM signal with mass of a DM particle labeled m_χ. The values of M_* used for the calculation for a given operator are shown in the table. The cross-sections are leading order, and the values are inclusive for $\ell = e, \mu, \tau$.

m_χ [GeV]	DM production σB[pb] D1 $M_* = 10$ GeV	D5d $M_* = 100$ GeV	D5c $M_* = 1$ TeV	D9 $M_* = 1$ TeV
1	438.6	72.19	0.0608	0.0966
100	331.9	70.80	0.0575	0.0870
200	201.2	58.84	0.0488	0.0695
400	64.56	32.91	0.0279	0.0365
1000	1.603	2.37	0.00192	0.00227
1300	0.0213	0.454	0.000351	0.000412

of interactions per bunch crossing observed in data, but are otherwise reconstructed in the same manner as data.

The $W \to \ell\nu$ and $Z \to \ell\ell$ cross-sections are calculated at next-to-next-to-leading-order (NNLO) with ZWPROD [49] using MSTW2008 NNLO PDFs. Consistent results are obtained using VRAP v0.9 [50] and FEWZ v3.1b2 [51, 52]. Higher order electroweak corrections are calculated with MCSANC [53]. Mass-dependent K-factors obtained from the ratios of the calculated NNLO cross-sections, with additional electroweak corrections, to the cross-sections of the generated samples are used to scale W^+, W^- and Z backgrounds separately. The $W' \to \ell\nu$ cross-sections are calculated in the same way, except that the electroweak corrections beyond final-state radiation are not included because the calculation for the SM W cannot be applied directly. Cross sections for $W^* \to \ell\nu$ are kept at LO due to the non-renormalizability of the model at higher orders in QCD. The $t\bar{t}$ cross-section is also calculated at NNLO including resummation of next-to-next-to-leading logarithmic (NNLL) soft gluon terms obtained with Top++ v2.0 [54–59] for a top quark mass of 172.5 GeV. The W'/W^* and DM particle signal cross sections are listed in table 1 and table 2, respectively. The most important background cross-sections are listed in table 3.

Table 3: Calculated values of σB for the leading backgrounds. The value for $t\bar{t} \to \ell X$ includes all final states with at least one lepton (e, μ or τ). The others are exclusive and are used for both $\ell = e$ and $\ell = \mu$. All calculations are NNLO except $t\bar{t}$ which is approximate-NNLO.

Process	σB [pb]
$W \to \ell\nu$	12190
$Z/\gamma^* \to \ell\ell$ ($m_{Z/\gamma^*} > 60$ GeV)	1120
$t\bar{t} \to \ell X$	137.3

Uncertainties on the W' and the W/Z background cross-sections are considered due to variations of the renormalization and factorization scales, PDF+α_s variations and PDF choice. The scale uncertainties are estimated by varying both the renormalization and factorization scales simultaneously up or down by a factor of two. The resulting maximum variation from the two fluctuations is taken as the symmetric scale uncertainty. The PDF+α_s uncertainty is evaluated using 90% CL eigenvector and 90% α_s variations of the nominal MSTW2008 NNLO PDF set. The result of this step is combined with the scale uncertainty in quadrature. The PDF choice uncertainty is evaluated by comparing the central values of the MSTW2008 NNLO , CT10 NNLO, NNPDF 2.3 NNLO [60], ABM11 5N NNLO [61] and HERAPDF 1.5 NNLO [62] PDF sets. The envelope provided by the last step and combination of the scale and PDF+α_s uncertainties is taken as the total uncertainty on the differential cross-section for the boson invariant mass. The PDF and α_s uncertainties on the $t\bar{t}$ cross-section are calculated using the PDF4LHC prescription [63] with the MSTW2008 68% CL NNLO, CT10 NNLO and NNPDF2.3 5f FFN PDF error sets added in quadrature to the scale uncertainty. The systematic uncertainty arising from the variation of the top mass by ±1 GeV is also added in quadrature.

An uncertainty for the beam energy is calculated for the Charged-Current Drell-Yan process with VRAP at NNLO using CT10 NNLO PDFs by taking a 0.66% uncertainty on the energy of each 4 TeV proton beam as determined from ref. [64]. The size of the uncertainty is observed to be about 0.1% at an invariant mass of 100 GeV, 2% at 2 TeV, and 6% at 3 TeV. Uncertainties are propagated to the $W \to \ell\nu$ samples, which constitute the dominant background, in order to derive an uncertainty in each signal region. The beam energy uncertainty is neglected in the calculation of the signal efficiency uncertainty.

Uncertainties are not reported on the cross-sections for W^* due to the breakdown of higher-order corrections for non-renormalizable models.

5 Event Selection

The primary vertex for each event is required to have at least three tracks with $p_{\mathrm{T}} > 0.4$ GeV and to have a longitudinal distance less than 200 mm from the centre of the collision region. There are on average 21 interactions per event in the data used for this analysis. The primary vertex is defined to be the one with the highest summed track p_{T}^2. Spurious tails in the missing E_{T} distribution, arising from calorimeter noise and other detector problems are suppressed by checking the quality of each reconstructed jet and discarding events containing reconstructed jets of poor quality, following description given in ref. [65]. In addition, the inner detector track associated with the electron or muon is required to be compatible with originating from the primary vertex, specifically to have transverse distance of closest approach $|d_0| < 1$ (0.2) mm and longitudinal distance at this point $|z_0| < 5$ (1) mm for the electron (muon). Events are required to have exactly one electron candidate or one muon candidate satisfying these requirements and passing identification criteria described in Section 3. In the electron channel, events with additional electrons passing the same identification criteria as for the candidate electron but with a lower E_{T} threshold of 20 GeV, are not considered. Similarly in the muon channel, events with additional muon candidates with p_{T} threshold of 20 GeV are discarded.

To suppress the QCD background, the lepton is required to be isolated. In the electron channel, the isolation energy is measured with the calorimeter in a cone $\Delta R = \sqrt{(\Delta\eta)^2 + (\Delta\varphi)^2} < 0.2$ around the electron track, and the requirement is $\Sigma E_{\mathrm{T}}^{\mathrm{calo}} < 0.007 \times E_{\mathrm{T}} + 5$ GeV, where the sum includes all calorimeter energy clusters in the cone excluding the core energy deposited by the electron. The sum is corrected to account for additional interactions and leakage of the electron energy outside this core. The scaling of the threshold with the electron E_{T} reduces the efficiency loss due to radiation from the electron at high E_{T}. In the muon channel, the isolation energy is measured using inner detector tracks with $p_{\mathrm{T}}^{\mathrm{trk}} > 1$ GeV in a cone $\Delta R < 0.3$ around the muon track. The isolation requirement is $\sum p_{\mathrm{T}}^{\mathrm{trk}} < 0.05 \times p_{\mathrm{T}}$, where the muon track is excluded from the sum. As in the electron channel, the scaling of the threshold with the muon p_{T} reduces the efficiency loss due to radiation from the muon at high p_{T}.

Missing E_{T} thresholds are imposed to further suppress the background from QCD and W+jets. In both channels, the threshold used for the charged lepton p_{T} is also applied to the missing E_{T}: $E_{\mathrm{T}}^{\mathrm{miss}} >$ 125 GeV for the electron channel and $E_{\mathrm{T}}^{\mathrm{miss}} > 45$ GeV for the muon channel.

The QCD background is evaluated using the *matrix method* [66] in both the electron and muon channels. In the electron channel, it constitutes about 2–4% of the total background at high m_{T}. Consistent results are obtained using the *inverted isolation* technique described in ref. [4]. In the muon channel, the QCD background constitutes about 1–3% of the total background at high m_{T}.

The same reconstruction and event selection are applied to both data and simulated samples. Figure 1 shows the p_{T}, $E_{\mathrm{T}}^{\mathrm{miss}}$, and m_{T} spectra for each channel after event selection for the data, for the expected background, and for three examples of W' signals at different masses. Prior to establishing if there is evidence for a signal, the agreement between data and predicted background is established for events with $m_{\mathrm{T}} < 252$ GeV, the lowest m_{T} threshold used to search for new physics. The optimization of m_{T} selection thresholds depending on the mass candidate is described below. The agreement between the data and expected background is good. Table 4 shows as an example how different sources contribute to the background for $m_{\mathrm{T}} > 1500$ GeV, the region used to search for a W' with a mass of 2000 GeV. The $W \to \ell\nu$ background is the dominant contribution for both the electron and muon channels.

Table 4: Expected numbers of events from the various background sources in each decay channel for $m_{\mathrm{T}} > 1500$ GeV, the region used to search for a W' with a mass of 2000 GeV. The $W \to \ell\nu$ and $Z \to \ell\ell$ rows include the expected contributions from the τ-lepton. The uncertainties are statistical.

	$e\nu$	$\mu\nu$
$W \to \ell\nu$	2.65 ± 0.10	2.28 ± 0.21
$Z \to \ell\ell$	0.00163 ± 0.00022	0.232 ± 0.005
diboson	0.27 ± 0.23	0.46 ± 0.23
top	0.0056 ± 0.0009	0.0017 ± 0.0001
multijet background	0.066 ± 0.019	0.046 ± 0.039
Total	2.99 ± 0.25	3.02 ± 0.31

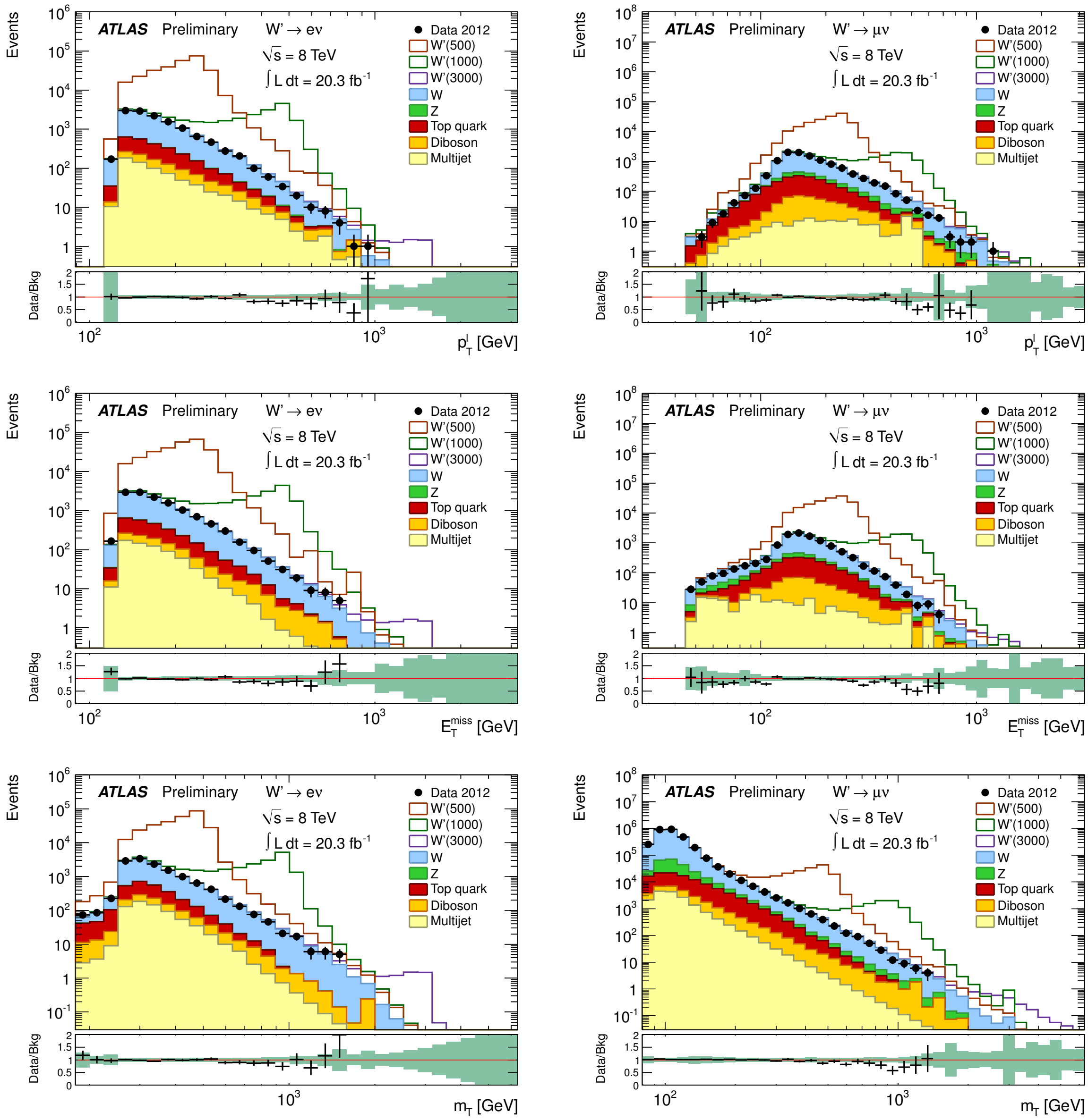

Figure 1: Spectra of lepton p_{T} (top), $E_{\mathrm{T}}^{\mathrm{miss}}$ (center) and m_{T} (bottom) for the electron (left) and muon (right) channels after the event selection. The spectra of p_{T} and $E_{\mathrm{T}}^{\mathrm{miss}}$ are shown with the requirement m_{T} > 252 GeV. The points represent data and the filled, stacked histograms show the predicted backgrounds. Open histograms are $W' \rightarrow \ell\nu$ signals added to the background with their masses in GeV indicated in parentheses in the legend. The signal and background samples are normalized using the integrated luminosity of the data and the NNLO cross-sections listed in tables 1 and 3, except for the multijet background which is estimated from data. The error bars on the data points are statistical. The ratio between the data and the total background prediction is shown below each of the distributions. The bands include systematic uncertainties on the background including the ones arising from the statistical uncertainty of the simulated samples.

6 Statistical Analysis and Systematics

A Bayesian analysis is performed to set limits on the studied processes. For each candidate mass and decay channel, events are counted above an m_{T} threshold, $m_{\mathrm{T}} > m_{\mathrm{Tmin}}$. The optimization of m_{Tmin} is done separately for $W' \to \ell\nu$ and $W^* \to \ell\nu$, resulting in separate thresholds. For each m_{W'/W^*}, the m_{Tmin} values are obtained in the electron and muon channels separately, but for simplicity the minimum one is used in both channels. A similar optimization is performed for setting the limits on DM production, and in this case a single m_{Tmin} is chosen for a given operator. The expected number of events in each channel is

$$N_{\mathrm{exp}} = \varepsilon_{\mathrm{sig}} L_{\mathrm{int}} \sigma B + N_{\mathrm{bg}}, \tag{2}$$

where L_{int} is the integrated luminosity of the data sample, $\varepsilon_{\mathrm{sig}}$ is the event selection efficiency that is the fraction of events that pass event selection criteria and have m_{T} above threshold, and N_{bg} is the expected number of background events. σB is the cross-section as defined in Section 1, and B is the branching fraction of W'/W^* decaying into lepton (electron or a muon) and a neutrino. $\varepsilon_{\mathrm{sig}}$ is calculated by applying the generator level requirement $m_{\ell\nu} > 0.4\, m_{W'}$ only in the denominator. This increases $\varepsilon_{\mathrm{sig}}$ by less than 1% relative to the $\varepsilon_{\mathrm{sig}}$ calculated by applying the same requirement in both the numerator and the denominator, except for the highest mass where the increase is 3%. For limits on DM production, total cross section times branching fraction is used. Using Poisson statistics, the likelihood to observe N_{obs} events is

$$\mathcal{L}(N_{\mathrm{obs}}|\sigma B) = \frac{(L_{\mathrm{int}}\varepsilon_{\mathrm{sig}}\sigma B + N_{\mathrm{bg}})^{N_{\mathrm{obs}}} e^{-(L_{\mathrm{int}}\varepsilon_{\mathrm{sig}}\sigma B + N_{\mathrm{bg}})}}{N_{\mathrm{obs}}!}. \tag{3}$$

Uncertainties are handled by introducing nuisance parameters θ_i, each with a probability density function (pdf) $g_i(\theta_i)$, and integrating the product of the Poisson likelihood with the pdfs. The integrated likelihood is

$$\mathcal{L}_B(N_{\mathrm{obs}}|\sigma B) = \int \mathcal{L}(N_{\mathrm{obs}}|\sigma B) \prod g_i(\theta_i) d\theta_i, \tag{4}$$

where a log-normal distribution is used for the $g_i(\theta_i)$. The nuisance parameters are taken to be: L_{int}, $\varepsilon_{\mathrm{sig}}$ and N_{bg}, with appropriate correlation between the first and the third parameters.

The measurements in the two decay channels are combined assuming the same branching fraction for each. Equation (4) remains valid with the Poisson likelihood replaced by the product of the Poisson likelihoods for the two channels. The electron and muon integrated luminosity measurements are fully correlated. For $W' \to \ell\nu$ the signal efficiencies and background levels are partly correlated with each other and between the two channels due to the full correlation of the cross section uncertainties. If these correlations are not included, the observed σB limits for the lowest mass points improve by 25%–30%, for the high-mass points $m_{W'} > 3000$ GeV by 10%, while the improvement for intermediate mass points is at a percent level. For W^* the background predictions are taken to be partly correlated between the two channels.

Bayes theorem gives the posterior probability that the signal has signal strength σB:

$$P_{\mathrm{post}}(\sigma B|N_{\mathrm{obs}}) = N \mathcal{L}_B(N_{\mathrm{obs}}|\sigma B)\, P_{\mathrm{prior}}(\sigma B) \tag{5}$$

where $P_{\mathrm{prior}}(\sigma B)$ is the assumed prior probability, here chosen to be one (that is flat in σB) for $\sigma B > 0$. The constant factor N normalizes the total probability to one. The posterior probability is evaluated for each mass and each decay channel and their combination, and then used to set a limit on σB.

The inputs for the evaluation of $\mathcal{L}_B$ (and hence P_{post}) are L_{int}, $\varepsilon_{\mathrm{sig}}$, N_{bg}, N_{obs} and the uncertainties on the first three. The uncertainties on $\varepsilon_{\mathrm{sig}}$ and N_{bg} account for experimental and theoretical systematic effects as well as the statistics of the simulation samples. The experimental systematic uncertainties include those on efficiencies for the electron or muon trigger, reconstruction and selection. Lepton momentum and missing E_{T} response, characterized by scale and resolution, are also included. Most of these

Table 5: Relative uncertainties on the event selection efficiency and background abundance for a W' with a mass of 2000 GeV. The efficiency uncertainties include contributions from the trigger, reconstruction and event selection. The last row gives the total relative uncertainties.

	$\varepsilon_{\mathrm{sig}}$		N_{bg}	
Source	$e\nu$	$\mu\nu$	$e\nu$	$\mu\nu$
Reco. and trig. efficiency	2.5%	4.1%	2.7%	4.1%
Lepton energy/momentum resolution	0.2%	1.4%	1.9%	18%
Lepton energy/momentum scale	1.2%	1.8%	3.5%	1.5%
$E_{\mathrm{T}}^{\mathrm{miss}}$ scale and resolution	0.1%	0.1%	1.2%	0.5%
Beam energy	-	-	2.8%	2.1%
Multijet background	-	-	2.2%	3.4%
Monte Carlo statistics	0.9%	1.3%	8.5%	10%
Cross-section (shape/level)	0.9%	0.8%	18%	15%
Total	3.1%	4.9%	21%	27%

performance metrics are measured at relatively low p_{T} and their values are extrapolated to the high-p_{T} regime relevant to this analysis. The uncertainties in these extrapolations are included but are too small to significantly affect the results. Table 5 summarizes the uncertainties on the event selection efficiencies and background levels for the $W' \to \ell\nu$ signal with $m_{W'} = 2000$ GeV using $m_{\mathrm{T}} > 1500$ GeV.

The inputs for the evaluation of $\mathcal{L}_B$ are listed in tables 6, 7 and 8. The uncertainties on $\varepsilon_{\mathrm{sig}}$ and N_{bg} account for all relevant experimental and theoretical effects except for the uncertainty on the integrated luminosity. The latter is included separately to allow for the correlation between signal and background. The table also lists the predicted numbers of signal events, N_{sig}, with their uncertainties accounting for the uncertainties in both $\varepsilon_{\mathrm{sig}}$ and the cross-section calculation. The maximum value for the signal selection efficiency is at $m_{W'} = 2000$ GeV. For lower masses, the efficiency falls because the relative m_{T} threshold, $m_{\mathrm{Tmin}}/m_{W'}$, increases to reduce the background level. The contribution from $W' \to \tau\nu$ with τ leptonically decaying has been neglected. It would increase signal strength by 2-3% for the highest masses. The background level is estimated for each mass by summing all the background sources.

Table 6: Inputs to the $W' \to \ell\nu$ σB limit calculations. The first three columns are the W' mass, m_T threshold and decay channel, respectively. The next two are the signal selection efficiency as defined in the text, ε_{sig}, and the prediction for the number of signal events, N_{sig}, obtained with this efficiency. The last two columns are the expected number of background events, N_{bg}, and the number of events observed in data, N_{obs}. The uncertainties on N_{sig} and N_{bg} include contributions from the uncertainties on the cross-sections but not from that on the integrated luminosity.

$m_{W'}$ [GeV]	m_{Tmin} [GeV]	channel	ε_{sig}	N_{sig}	N_{bg}	N_{obs}
300	252	$e\nu$	0.230 ± 0.009	685000 ± 28000	12900 ± 830	12717
		$\mu\nu$	0.186 ± 0.007	553000 ± 21000	11300 ± 780	10954
400	336	$e\nu$	0.323 ± 0.012	325000 ± 12000	5280 ± 370	5176
		$\mu\nu$	0.195 ± 0.008	196000 ± 7500	3490 ± 250	3324
500	423	$e\nu$	0.330 ± 0.013	141000 ± 5700	2070 ± 160	2017
		$\mu\nu$	0.189 ± 0.007	81000 ± 3200	1370 ± 100	1223
600	474	$e\nu$	0.404 ± 0.014	83600 ± 2800	1260 ± 100	1214
		$\mu\nu$	0.233 ± 0.009	48100 ± 1900	827 ± 66	721
750	597	$e\nu$	0.402 ± 0.013	33200 ± 1100	456 ± 47	414
		$\mu\nu$	0.231 ± 0.009	19100 ± 750	305 ± 31	256
1000	796	$e\nu$	0.398 ± 0.013	9130 ± 290	116 ± 16	101
		$\mu\nu$	0.226 ± 0.010	5190 ± 220	84 ± 11	59
1250	1002	$e\nu$	0.396 ± 0.012	2980 ± 92	35.3 ± 5.8	34
		$\mu\nu$	0.219 ± 0.009	1650 ± 71	28.3 ± 4.6	19
1500	1191	$e\nu$	0.402 ± 0.013	1110 ± 35	13.2 ± 2.5	14
		$\mu\nu$	0.221 ± 0.010	608 ± 28	10.9 ± 2.3	6
1750	1416	$e\nu$	0.372 ± 0.012	397 ± 12	4.56 ± 0.92	5
		$\mu\nu$	0.201 ± 0.01	215 ± 11	4.3 ± 1.1	0
2000	1500	$e\nu$	0.431 ± 0.013	183.0 ± 5.6	2.99 ± 0.62	3
		$\mu\nu$	0.231 ± 0.011	98.1 ± 4.8	3.02 ± 0.81	0
2250	1683	$e\nu$	0.416 ± 0.014	71.5 ± 2.3	1.38 ± 0.33	0
		$\mu\nu$	0.220 ± 0.012	37.9 ± 2.0	1.44 ± 0.33	0
2500	1888	$e\nu$	0.381 ± 0.015	27.1 ± 1.1	0.43 ± 0.10	0
		$\mu\nu$	0.203 ± 0.012	14.4 ± 0.9	0.61 ± 0.15	0
2750	1888	$e\nu$	0.417 ± 0.022	12.30 ± 0.64	0.43 ± 0.10	0
		$\mu\nu$	0.225 ± 0.015	6.61 ± 0.44	0.61 ± 0.15	0
3000	1888	$e\nu$	0.425 ± 0.037	5.32 ± 0.46	0.43 ± 0.10	0
		$\mu\nu$	0.234 ± 0.022	2.93 ± 0.27	0.61 ± 0.15	0
3250	1888	$e\nu$	0.405 ± 0.066	2.21 ± 0.36	0.43 ± 0.10	0
		$\mu\nu$	0.226 ± 0.036	1.24 ± 0.20	0.61 ± 0.15	0
3500	1888	$e\nu$	0.368 ± 0.100	0.92 ± 0.25	0.43 ± 0.10	0
		$\mu\nu$	0.210 ± 0.052	0.52 ± 0.13	0.61 ± 0.15	0
3750	1888	$e\nu$	0.331 ± 0.091	0.40 ± 0.11	0.43 ± 0.10	0
		$\mu\nu$	0.193 ± 0.045	0.236 ± 0.055	0.61 ± 0.15	0
4000	1888	$e\nu$	0.310 ± 0.071	0.197 ± 0.045	0.43 ± 0.10	0
		$\mu\nu$	0.189 ± 0.035	0.120 ± 0.022	0.61 ± 0.15	0

Table 7: Inputs to the $W^* \to \ell\nu$ σB limit calculations. The columns are as for table 6.

m_{W^*} [GeV]	m_{Tmin} [GeV]	channel	$\varepsilon_{\mathrm{sig}}$	N_{sig}	N_{bg}	N_{obs}
400	317	$e\nu$	0.196 ± 0.010	150000 ± 7300	6630 ± 450	6448
		$\mu\nu$	0.111 ± 0.005	85600 ± 3700	4420 ± 320	4240
500	377	$e\nu$	0.246 ± 0.011	82400 ± 3600	3320 ± 230	3275
		$\mu\nu$	0.140 ± 0.006	46800 ± 1900	2210 ± 160	2014
600	448	$e\nu$	0.257 ± 0.011	42100 ± 1800	1630 ± 130	1582
		$\mu\nu$	0.144 ± 0.006	23500 ± 970	1080 ± 82	941
750	564	$e\nu$	0.248 ± 0.010	16300 ± 690	593 ± 57	524
		$\mu\nu$	0.143 ± 0.006	9400 ± 400	388 ± 37	322
1000	710	$e\nu$	0.302 ± 0.013	5530 ± 230	203 ± 25	177
		$\mu\nu$	0.174 ± 0.007	3180 ± 130	143 ± 17	110
1250	843	$e\nu$	0.337 ± 0.013	2040 ± 80	86 ± 12	79
		$\mu\nu$	0.191 ± 0.008	1160 ± 51	65.5 ± 8.6	40
1500	1062	$e\nu$	0.296 ± 0.011	655 ± 25	25.8 ± 4.4	26
		$\mu\nu$	0.164 ± 0.007	363 ± 16	20.9 ± 3.8	12
1750	1191	$e\nu$	0.324 ± 0.013	274 ± 11	13.2 ± 2.5	14
		$\mu\nu$	0.182 ± 0.009	154.0 ± 7.5	10.9 ± 2.3	6
2000	1337	$e\nu$	0.342 ± 0.013	114.0 ± 4.4	6.8 ± 1.3	9
		$\mu\nu$	0.187 ± 0.010	62.4 ± 3.2	5.8 ± 1.4	3
2250	1416	$e\nu$	0.391 ± 0.014	52.4 ± 1.9	4.56 ± 0.92	5
		$\mu\nu$	0.204 ± 0.010	27.3 ± 1.4	4.3 ± 1.1	0
2500	1683	$e\nu$	0.338 ± 0.013	18.30 ± 0.69	1.38 ± 0.33	0
		$\mu\nu$	0.179 ± 0.010	9.68 ± 0.52	1.44 ± 0.33	0
2750	1888	$e\nu$	0.323 ± 0.012	7.07 ± 0.27	0.43 ± 0.10	0
		$\mu\nu$	0.162 ± 0.011	3.54 ± 0.24	0.61 ± 0.15	0
3000	1888	$e\nu$	0.384 ± 0.014	3.38 ± 0.12	0.43 ± 0.10	0
		$\mu\nu$	0.186 ± 0.011	1.640 ± 0.096	0.61 ± 0.15	0
3250	1888	$e\nu$	0.440 ± 0.015	1.560 ± 0.054	0.43 ± 0.10	0
		$\mu\nu$	0.220 ± 0.013	0.779 ± 0.047	0.61 ± 0.15	0
3500	1888	$e\nu$	0.479 ± 0.016	0.685 ± 0.023	0.43 ± 0.10	0
		$\mu\nu$	0.232 ± 0.014	0.332 ± 0.020	0.61 ± 0.15	0
3750	1888	$e\nu$	0.508 ± 0.017	0.294 ± 0.010	0.43 ± 0.10	0
		$\mu\nu$	0.250 ± 0.015	0.144 ± 0.010	0.61 ± 0.15	0
4000	1888	$e\nu$	0.505 ± 0.016	0.1200 ± 0.0039	0.43 ± 0.10	0
		$\mu\nu$	0.251 ± 0.016	0.0595 ± 0.0037	0.61 ± 0.15	0

Table 8: Inputs to the limit calculations on pair production of DM particles for the operators D1, D5d, D5c and D9. Expected number of signal events for each operator is calculated for a different value of mass scale, notably $M_* = 10$ GeV for D1, $M_* = 100$ GeV for D5d, and $M_* = 1$ TeV for operators D9 and D5c. The columns are as for table 6, except $\varepsilon_{\rm sig}$ is inclusive efficiency, and m_χ is the mass of DM particle.

m_χ [GeV]	$m_{\rm Tmin}$ [GeV]	channel	$\varepsilon_{\rm sig}$	$N_{\rm sig}$		$N_{\rm bg}$	$N_{\rm obs}$
D1 Operator							
1	796	$e\nu$	0.0294 ± 0.0024	87200 ± 7000	$e\nu$	116 ± 16	101
		$\mu\nu$	0.0177 ± 0.0016	52500 ± 4800	$\mu\nu$	84 ± 11	59
100		$e\nu$	0.0396 ± 0.0026	88900 ± 5800			
		$\mu\nu$	0.0252 ± 0.0023	56600 ± 5100			
200		$e\nu$	0.0484 ± 0.0032	65800 ± 4400			
		$\mu\nu$	0.0293 ± 0.0023	39900 ± 3100			
400		$e\nu$	0.0709 ± 0.0036	30900 ± 1600			
		$\mu\nu$	0.0398 ± 0.0027	17300 ± 1200			
1000		$e\nu$	0.0989 ± 0.0046	1070 ± 50			
		$\mu\nu$	0.0621 ± 0.0038	673 ± 41			
1300		$e\nu$	0.0963 ± 0.0046	138 ± 6.6			
		$\mu\nu$	0.0522 ± 0.0032	75.1 ± 4.6			
D5d Operator							
1	597	$e\nu$	0.0148 ± 0.0015	7230 ± 740	$e\nu$	456 ± 47	414
		$\mu\nu$	0.0080 ± 0.0011	3890 ± 520	$\mu\nu$	305 ± 31	256
100		$e\nu$	0.0158 ± 0.0017	7580 ± 820			
		$\mu\nu$	0.0096 ± 0.0012	4600 ± 560			
200		$e\nu$	0.0147 ± 0.0015	5850 ± 590			
		$\mu\nu$	0.0086 ± 0.0011	3420 ± 420			
400		$e\nu$	0.0191 ± 0.0019	4220 ± 420			
		$\mu\nu$	0.0113 ± 0.0013	2490 ± 290			
1000		$e\nu$	0.0281 ± 0.0022	450 ± 36			
		$\mu\nu$	0.0177 ± 0.0017	283 ± 27			
1300		$e\nu$	0.0291 ± 0.0022	89.3 ± 6.8			
		$\mu\nu$	0.0167 ± 0.0016	51.1 ± 4.9			
D5c Operator							
1	843	$e\nu$	0.0737 ± 0.0039	30.3 ± 1.6	$e\nu$	86 ± 12	79
		$\mu\nu$	0.0435 ± 0.0029	17.9 ± 1.2	$\mu\nu$	65.5 ± 8.6	40
100		$e\nu$	0.0798 ± 0.0041	31.1 ± 1.6			
		$\mu\nu$	0.0437 ± 0.0031	17.0 ± 1.2			
200		$e\nu$	0.0762 ± 0.0038	25.1 ± 1.3			
		$\mu\nu$	0.0461 ± 0.0030	15.2 ± 1.0			
400		$e\nu$	0.0857 ± 0.0043	16.2 ± 0.8			
		$\mu\nu$	0.0532 ± 0.0032	10.0 ± 0.6			
1000		$e\nu$	0.0987 ± 0.0045	1.28 ± 0.06			
		$\mu\nu$	0.0636 ± 0.0036	0.82 ± 0.05			
1300		$e\nu$	0.1010 ± 0.0050	0.24 ± 0.01			
		$\mu\nu$	0.0589 ± 0.0035	0.14 ± 0.01			
D9 Operator							
1	843	$e\nu$	0.0851 ± 0.0044	55.5 ± 2.9	$e\nu$	86 ± 12	79
		$\mu\nu$	0.0517 ± 0.0031	33.8 ± 2.0	$\mu\nu$	65.5 ± 8.6	40
100		$e\nu$	0.0950 ± 0.0046	55.8 ± 2.7			
		$\mu\nu$	0.0529 ± 0.0032	31.1 ± 1.9			
200		$e\nu$	0.1040 ± 0.0050	48.9 ± 2.3			
		$\mu\nu$	0.0553 ± 0.0034	26.0 ± 1.6			
400		$e\nu$	0.1029 ± 0.0050	25.5 ± 1.2			
		$\mu\nu$	0.0578 ± 0.0034	14.3 ± 0.85			
1000		$e\nu$	0.1061 ± 0.0049	1.63 ± 0.08			
		$\mu\nu$	0.0615 ± 0.0037	0.94 ± 0.06			
1300		$e\nu$	0.1020 ± 0.0046	0.29 ± 0.01			
		$\mu\nu$	0.0573 ± 0.0034	0.16 ± 0.01			

7 Results

Tables 9 and 10 and figure 2 present the 95% CL observed limits on σB for both $W' \to \ell\nu$ and $W^* \to \ell\nu$ in the electron channel, the muon channel and their combination. The tables also give the limits obtained without systematic uncertainties and with various subsets. The uncertainties on the signal selection efficiency have very little effect on the final limits, and the background-level and luminosity uncertainties are important only for the lowest masses. The figure also shows the expected limits and the theoretical σB for a W' and for a W^* of the same width.

Table 9: Observed upper limits on W' and W^* σB for masses up to 2000 GeV. The first column is the W'/W^* mass and the following are the 95% CL limits for W' with headers indicating the nuisance parameters for which uncertainties are included: S for the event selection efficiency ($\varepsilon_{\mathrm{sig}}$), B for the background level (N_{bg}), and L for the integrated luminosity (L_{int}). The column labeled SBL includes all uncertainties neglecting correlations. Results are also presented including correlation of the signal and background cross-sections uncertainties, as well as correlation for background cross-section uncertainties for the combined limits ($\mathrm{SB_c}$, $\mathrm{SB_cL}$). The last two columns are the limits for W^* without the nuisance parameters and including all nuisance parameters with correlations.

m_{W'/W^*} [GeV]	channel	95% CL limit on σB [fb]							
		W'						W^*	
		none	S	SB	SBL	$\mathrm{SB_c}$	$\mathrm{SB_cL}$	none	$\mathrm{SB_cL}$
300	e	28.7	28.8	305	342	305	342		
	μ	23.5	23.6	329	366	329	366		
	$e\mu$	14.6	14.6	220	270	291	332		
400	e	13.9	13.9	95.3	105	95.4	105	20.7	204
	μ	12.8	12.8	92.6	103	92.6	103	26.0	234
	$e\mu$	7.58	7.59	64.3	77.5	84.5	95.7	12.8	198
500	e	9.01	9.04	39.3	42.8	39.4	42.9	17.3	88.1
	μ	6.46	6.48	31.9	35.2	31.9	35.4	10.8	79.8
	$e\mu$	4.25	4.26	23.1	27.6	31.0	35.0	7.67	79.1
600	e	5.58	5.59	20.0	21.6	20.1	21.7	10.4	44.9
	μ	4.37	4.39	16.1	17.6	16.2	17.7	7.23	34.1
	$e\mu$	2.76	2.76	11.5	13.6	16.2	18.0	4.81	35.3
750	e	2.88	2.89	8.36	8.79	8.41	8.86	4.23	15.3
	μ	3.31	3.32	8.08	8.52	8.13	8.58	5.29	15.2
	$e\mu$	1.71	1.71	5.19	5.74	7.18	7.67	2.52	13.4
1000	e	1.79	1.79	3.19	3.28	3.22	3.31	2.69	6.11
	μ	1.85	1.86	2.89	2.98	2.93	3.01	3.09	6.15
	$e\mu$	1.02	1.02	1.86	1.96	2.47	2.57	1.59	5.11
1250	e	1.56	1.56	1.97	2.00	1.98	2.01	2.29	3.67
	μ	1.55	1.55	1.89	1.92	1.91	1.94	1.78	2.60
	$e\mu$	0.946	0.947	1.24	1.27	1.45	1.48	1.16	2.56
1500	e	1.19	1.19	1.31	1.32	1.31	1.32	1.99	2.39
	μ	1.13	1.14	1.24	1.25	1.24	1.25	1.71	2.04
	$e\mu$	0.725	0.726	0.814	0.825	0.886	0.896	1.14	1.62
1750	e	0.871	0.874	0.897	0.901	0.900	0.904	1.48	1.63
	μ	0.735	0.739	0.739	0.742	0.741	0.744	1.37	1.51
	$e\mu$	0.471	0.471	0.482	0.486	0.502	0.506	0.890	1.09
2000	e	0.617	0.619	0.629	0.631	0.631	0.633	1.34	1.40
	μ	0.639	0.642	0.642	0.645	0.644	0.646	1.18	1.25
	$e\mu$	0.356	0.356	0.361	0.363	0.370	0.372	0.831	0.918

The numbers of observed events are generally in good agreement with the expected numbers of

Table 10: Observed upper limits on W' and W^* σB for masses above 2000 GeV. The columns are as for table 9.

m_{W'/W^*} [GeV]	channel	95% CL limit on σB [fb]							
		W'						W^*	
		none	S	SB	SBL	SB$_c$	SB$_c$L	none	SB$_c$L
2250	e	0.356	0.357	0.357	0.357	0.358	0.359	0.829	0.858
	μ	0.672	0.675	0.675	0.677	0.677	0.679	0.725	0.732
	$e\mu$	0.233	0.233	0.233	0.234	0.234	0.235	0.456	0.487
2500	e	0.388	0.389	0.389	0.390	0.390	0.391	0.437	0.440
	μ	0.729	0.735	0.735	0.736	0.737	0.739	0.827	0.834
	$e\mu$	0.253	0.254	0.254	0.254	0.255	0.256	0.286	0.288
2750	e	0.354	0.356	0.356	0.357	0.358	0.358	0.458	0.460
	μ	0.657	0.663	0.663	0.665	0.667	0.668	0.914	0.925
	$e\mu$	0.230	0.231	0.231	0.231	0.233	0.234	0.305	0.307
3000	e	0.348	0.354	0.354	0.354	0.356	0.357	0.385	0.387
	μ	0.633	0.643	0.643	0.645	0.649	0.651	0.795	0.802
	$e\mu$	0.225	0.226	0.226	0.227	0.231	0.232	0.260	0.261
3250	e	0.366	0.385	0.385	0.386	0.391	0.392	0.336	0.337
	μ	0.655	0.688	0.688	0.689	0.699	0.701	0.673	0.680
	$e\mu$	0.235	0.240	0.240	0.241	0.254	0.255	0.224	0.225
3500	e	0.402	0.462	0.462	0.463	0.473	0.474	0.309	0.310
	μ	0.704	0.789	0.789	0.791	0.810	0.812	0.637	0.643
	$e\mu$	0.256	0.271	0.271	0.272	0.305	0.306	0.208	0.209
3750	e	0.447	0.516	0.516	0.517	0.528	0.529	0.291	0.292
	μ	0.765	0.849	0.849	0.851	0.870	0.872	0.592	0.598
	$e\mu$	0.282	0.299	0.299	0.299	0.336	0.337	0.195	0.196
4000	e	0.477	0.528	0.528	0.529	0.539	0.540	0.293	0.294
	μ	0.781	0.836	0.836	0.838	0.853	0.855	0.590	0.595
	$e\mu$	0.296	0.308	0.308	0.309	0.336	0.337	0.195	0.196

Table 11: Lower limits on the W' and W^* masses. The first column is the decay channel ($e\nu$, $\mu\nu$ or both combined) and the following give the expected (Exp.) and observed (Obs.) mass limits.

	$m_{W'}$ [TeV]		m_{W^*} [TeV]	
decay	Exp.	Obs.	Exp.	Obs.
$e\nu$	3.15	3.15	3.04	3.04
$\mu\nu$	2.98	2.98	2.80	2.80
both	3.19	3.27	3.08	3.17

background events for all mass bins. None of the observations for any mass point in either channel or their combination show an excess above background, so there is no evidence for the observation of $W' \to \ell\nu$ or $W^* \to \ell\nu$. A deficit of the number of observed events with respect to the expected numbers of background events is observed in the muon channel. This deficit is at most at 2σ local significance.

The intersection between the central theoretical prediction and the observed limits provides the 95% CL lower limits on the mass. Table 11 presents the expected and observed W' and W^* mass limits for the electron and muon decay channels and their combination. The band around the theoretical prediction indicates the PDF uncertainty given in table 1. The mass limits for the W' decrease by 100 GeV if the intersection between the lower theoretical prediction and observed limit is used. The uncertainties on $\varepsilon_{\mathrm{sig}}$, N_{bg} and L_{int} have a marginal impact on the derived mass limits.

The results above are obtained using log normal distributions for the probability density functions of

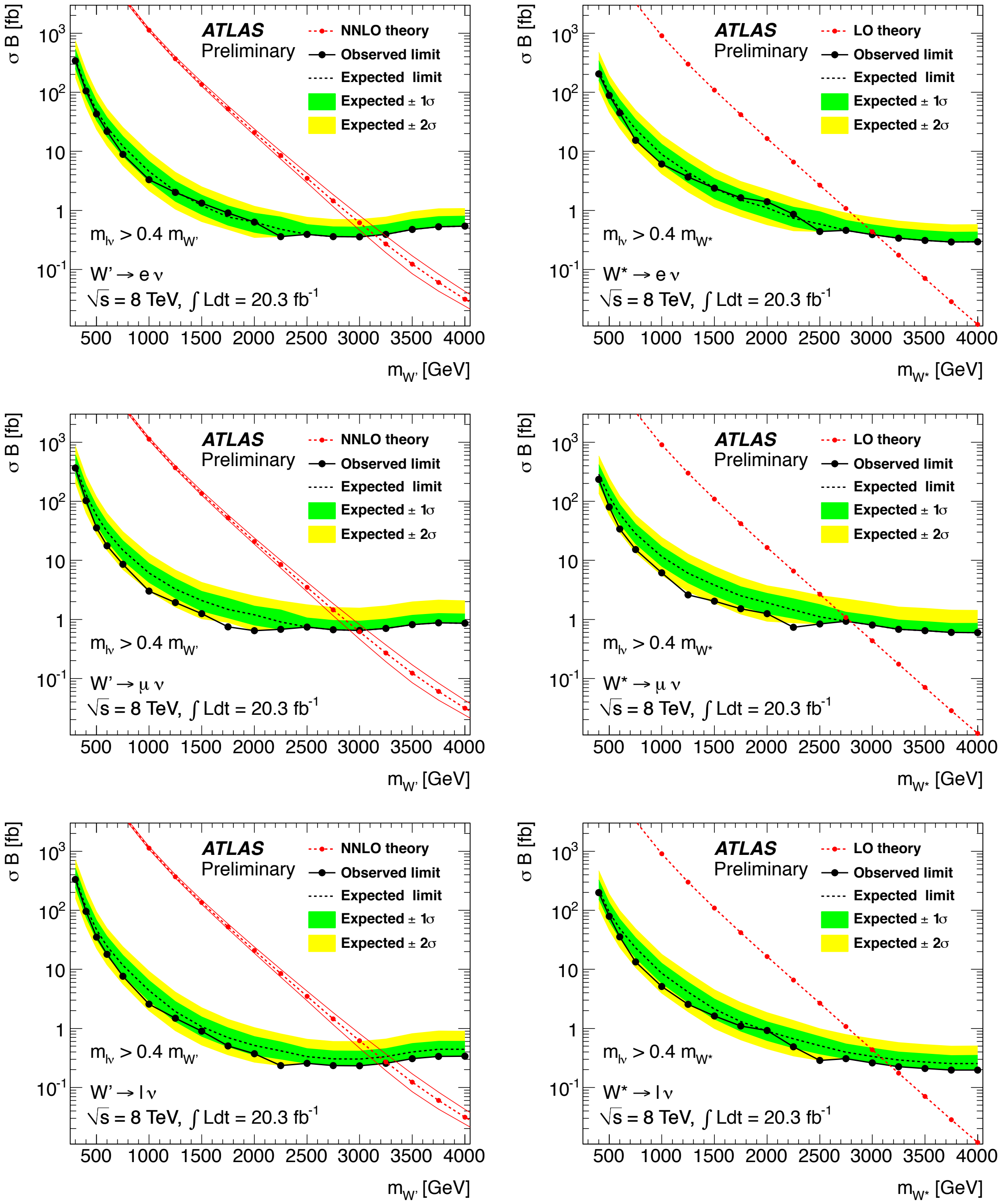

Figure 2: Observed and expected limits on σB for W' (left) and W^* (right) in the electron channel (top), muon channel (center) and the combination (bottom) assuming the same branching fraction for both channels. The predicted values for σB and their uncertainties (except for W^*) are also shown. The uncertainties on the W' cross-sections are calculated from variations of the MSTW 2008 NNLO PDF at 90% CL.

nuisance parameters. The Gaussian distribution of the background uncertainties would lead to weaker cross-section limits of up to 10%, with only marginal impact on the mass limit.

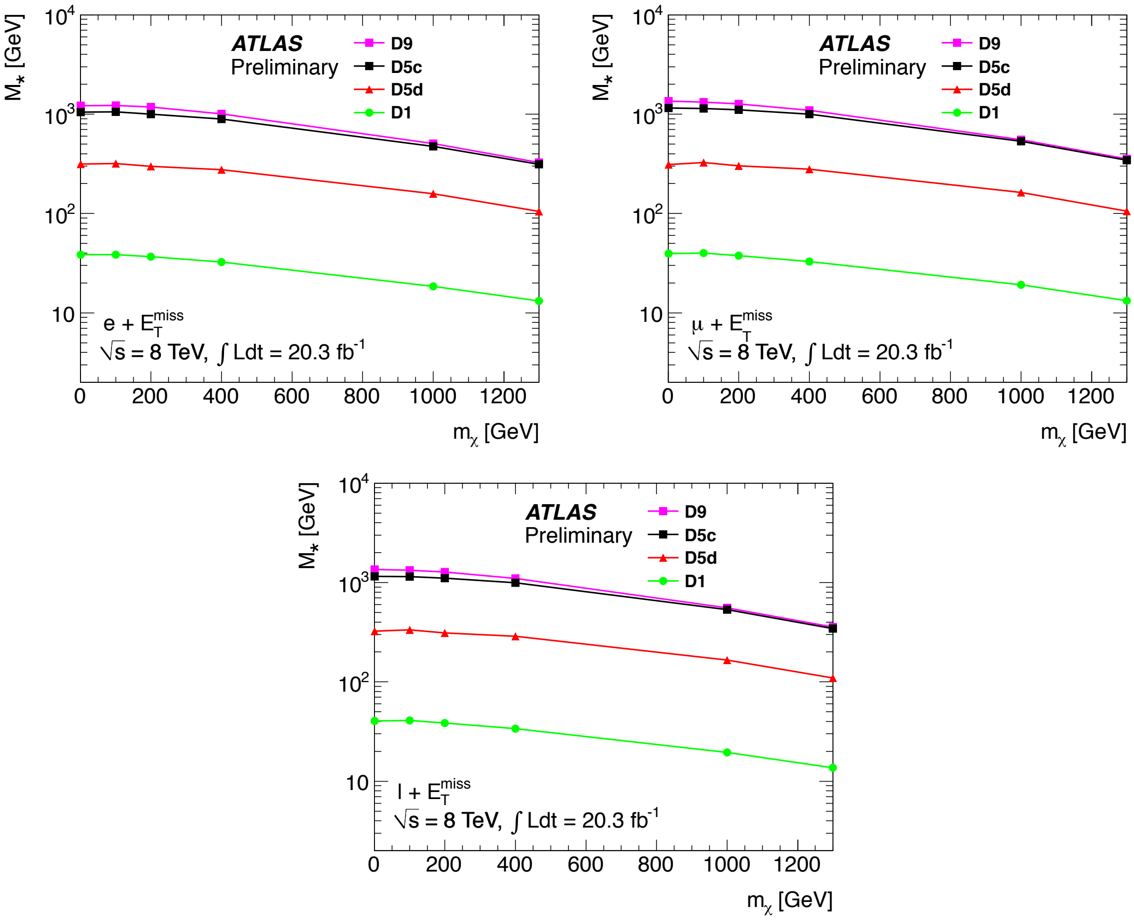

Figure 3: Observed limits on M_* as a function of the mass of the DM particle (m_χ) at 95% CL in the electron channel (top left), muon channel (top right) and the combinations (bottom), or various operators as described in the text. For each operator, the values below the corresponding line are excluded. No signal samples are generated for masses below 1 GeV but the limits are expected to be stable down to arbitrarily small values.

The mass limits presented here are a significant improvement over those reported in previous ATLAS analyses [4–6] and are similar to the most recent results from CMS [3, 67].

Finally the results for DM particle pair production search, namely the 95% CL exclusion regions for M_* versus m_χ, can be found in figure 3. A corresponding set of limits at 90% CL are reported in [15] where hadronic decays of W and Z bosons are considered.

8 Conclusions

A search is presented for new high-mass states decaying to a lepton (electron or muon) plus missing transverse momentum using 20.3 fb^{-1} of proton-proton collision data at $\sqrt{s}$ = 8 TeV recorded with the ATLAS experiment at the Large Hadron Collider. No significant excess beyond SM expectations is observed. Limits on σB are presented. A W' with SSM couplings is excluded for masses below 3.27 TeV at 95% CL. The exclusion for W^* with equivalent couplings is 3.17 TeV. Limits on production of pairs of weakly interacting DM particles in events with a leptonically decaying W are set on the mass scale M_* of the unknown mediating interaction.

References

[1] T. Aaltonen et al., CDF Collaboration, *Search for a New Heavy Gauge Boson W' with Electron + missing E_T Event Signature in $p\bar{p}$ collisions at* $\sqrt{s}$ *= 1.96 TeV*, Phys. Rev. D **83** (2011) 031102, arXiv:1012.5145 [hep-ex].

[2] CMS Collaboration, *Search for leptonic decays of W' in pp collisions at* $\sqrt{s}$ = 7 TeV, J. High Energy Phys. **1208** (2012) 023, arXiv:1204.4764 [hep-ex].

[3] CMS Collaboration, *Search for new physics in final states with a lepton and missing transverse energy in pp collisions at the LHC*, Phys. Rev. D **87** (2013) 072005, arXiv:1302.2812 [hep-ex].

[4] ATLAS Collaboration, *Search for high-mass states with one lepton plus missing transverse momentum in proton-proton collisions at* $\sqrt{s}$ = 7 TeV *with the ATLAS detector*, Phys. Lett. B **701** (2011) 50, arXiv:1103.1391 [hep-ex].

[5] ATLAS Collaboration, *Search for a heavy gauge boson decaying to a charged lepton and a neutrino in 1 fb^{-1} of pp collisions at* $\sqrt{s}$ *= 7 TeV using the ATLAS detector*, Phys. Lett. B **705** (2011) 28–46, arXiv:1108.1316 [hep-ex].

[6] ATLAS Collaboration, *ATLAS search for a heavy gauge boson decaying to a charged lepton and a neutrino in pp collisions at* $\sqrt{s}$ = 7 TeV, The European Physical Journal C **72** no. 12, (2012) 1–23, arXiv:1209.4446 [hep-ex].

[7] G. Altarelli, B. Mele, and M. Ruiz-Altaba, *Searching for new heavy vector bosons in $p\bar{p}$ colliders*, Z. Phys. C **45** (1989) 109.

[8] M. Chizhov, V. Bednyakov, and J. Budagov, *Proposal for chiral bosons search at LHC via their unique new signature*, Phys.Atom.Nucl. **71** (2008) 2096–2100, arXiv:0801.4235 [hep-ph].

[9] M. Chizhov and G. Dvali, *Origin and Phenomenology of Weak-Doublet Spin-1 Bosons*, Phys Lett. B **703** (2011) 593–598, arXiv:0908.0924 [hep-ph].

[10] T. Aaltonen et al., CDF Collaboration, *A Search for dark matter in events with one jet and missing transverse energy in $p\bar{p}$ collisions at* $\sqrt{s}$ = 1.96 *TeV*, Phys.Rev.Lett. **108** (2012) 211804, arXiv:1203.0742 [hep-ex].

[11] ATLAS Collaboration, *Search for dark matter candidates and large extra dimensions in events with a jet and missing transverse momentum with the ATLAS detector*, J.High Energy Phys. **1304** (2013) 075, arXiv:1210.4491 [hep-ex].

[12] CMS Collaboration, *Search for dark matter and large extra dimensions in monojet events in pp collisions at* $\sqrt{s}$ = 7 TeV, J. High Energy Phys. **1209** (2012) 094, arXiv:1206.5663 [hep-ex].

[13] ATLAS Collaboration, *Search for dark matter candidates and large extra dimensions in events with a photon and missing transverse momentum in pp collision data at* $\sqrt{s}$ = 7 TeV *with the ATLAS detector*, Phys. Rev. Lett. **110** (2013) 011802, arXiv:1209.4625 [hep-ex].

[14] CMS Collaboration, *Search for dark matter and large extra dimensions in pp collisions yielding a photon and missing transverse energy*, Phys. Rev. Lett. **108** (2012) 261803, arXiv:1204.0821 [hep-ex].

[15] ATLAS Collaboration, *Search for dark matter in events with a hadronically decaying W or Z boson and missing transverse momentum in pp collisions at $\sqrt{s}$=8 TeV with the ATLAS detector*, Phys.Rev.Lett. **112** (2014) 041802, `arXiv:1309.4017 [hep-ex]`.

[16] Y. Bai and T. M. Tait, *Searches with Mono-Leptons*, Phys.Lett. **B723** (2013) 384–387, `arXiv:1208.4361 [hep-ph]`.

[17] ATLAS Collaboration, *Measurement of ZZ production in pp collisions at $\sqrt{s}$ = 7 TeV and limits on anomalous ZZZ and ZZγ couplings with the ATLAS detector*, J.High Energy Phys. **1303** (2013) 128, `arXiv:1211.6096 [hep-ex]`.

[18] L. Carpenter, A. Nelson, C. Shimmin, T. Tait, and D. Whiteson, *Collider searches for dark matter in events with a Z boson and missing energy*, Phys. Rev. D **87** (2013) 074005, `arXiv:1212.3352 [hep-ex]`.

[19] Q.-H. Cao, C.-R. Chen, C. S. Li, and H. Zhang, *Effective Dark Matter Model: Relic density, CDMS II, Fermi LAT and LHC*, J.High Energy Phys. **1108** (2011) 018, `arXiv:0912.4511 [hep-ph]`.

[20] M. Beltran, D. Hooper, E. W. Kolb, Z. A. Krusberg, and T. M. Tait, *Maverick dark matter at colliders*, J.High Energy Phys. **1009** (2010) 037, `arXiv:1002.4137 [hep-ph]`.

[21] J. Goodman, M. Ibe, A. Rajaraman, W. Shepherd, T. M. Tait, et al., *Constraints on Light Majorana dark Matter from Colliders*, Phys.Lett. **B695** (2011) 185–188, `arXiv:1005.1286 [hep-ph]`.

[22] Y. Bai, P. J. Fox, and R. Harnik, *The Tevatron at the Frontier of Dark Matter Direct Detection*, J.High Energy Phys. **1012** (2010) 048, `arXiv:1005.3797 [hep-ph]`.

[23] J. Goodman, M. Ibe, A. Rajaraman, W. Shepherd, T. M. Tait, et al., *Constraints on Dark Matter from Colliders*, Phys.Rev. **D82** (2010) 116010, `arXiv:1008.1783 [hep-ph]`.

[24] A. Rajaraman, W. Shepherd, T. M. Tait, and A. M. Wijangco, *LHC Bounds on Interactions of Dark Matter*, Phys.Rev. **D84** (2011) 095013, `arXiv:1108.1196 [hep-ph]`.

[25] P. J. Fox, R. Harnik, J. Kopp, and Y. Tsai, *Missing Energy Signatures of Dark Matter at the LHC*, Phys.Rev. **D85** (2012) 056011, `arXiv:1109.4398 [hep-ph]`.

[26] K. Cheung, P.-Y. Tseng, Y.-L. S. Tsai, and T.-C. Yuan, *Global Constraints on Effective Dark Matter Interactions: Relic Density, Direct Detection, Indirect Detection, and Collider*, JCAP **1205** (2012) 001, `arXiv:1201.3402 [hep-ph]`.

[27] R. Cotta, J. Hewett, M. Le, and T. Rizzo, *Bounds on Dark Matter Interactions with Electroweak Gauge Bosons*, Phys.Rev. **D88** (2013) 116009, `arXiv:1210.0525 [hep-ph]`.

[28] O. Buchmueller, M. J. Dolan, and C. McCabe, *Beyond Effective Field Theory for Dark Matter Searches at the LHC*, J.High Energy Phys. **1401** (2014) 025, `arXiv:1308.6799 [hep-ph]`.

[29] G. Busoni, A. De Simone, E. Morgante, and A. Riotto, *On the Validity of the Effective Field Theory for Dark Matter Searches at the LHC*, Phys.Lett. **B728** (2014) 412–421, `arXiv:1307.2253 [hep-ph]`.

[30] ATLAS Collaboration, *ATLAS Experiment at the CERN Large Hadron Collider*, JINST **3** (2008) S08003.

[31] ATLAS Collaboration, *Electron performance measurements with the ATLAS detector using the 2010 LHC proton-proton collision data*, Eur. Phys. J. C **72** (2012) 1909, `arXiv:1110.3174 [hep-ex]`.

[32] ATLAS Collaboration, *Performance of missing transverse momentum reconstruction in proton-proton collisions at 7 TeV in ATLAS*, Eur. Phys. J. C **72** (2012) 1844, `arXiv:1108.5602 [hep-ex]`.

[33] ATLAS Collaboration, *Improved luminosity determination in pp collisions at $\sqrt{s}$ = 7 TeV using the ATLAS detector at the LHC*, Eur. Phys. J. C **73** (2013) 2518, `arXiv:1302.4393 [hep-ex]`.

[34] T. Sjostrand, S. Mrenna, and P. Skands, *PYTHIA 6.4 physics and manual*, J. High Energy Phys. **0605** (2006) 026.

[35] A. Martin, W. Stirling, R. Thorne, and G. Watt, *Parton distributions for the LHC*, Eur. Phys. J. C **63** (2009) 189, `arXiv:0901.0002 [hep-ph]`.

[36] A. Belyaev, N. D. Christensen, and A. Pukhov, *CalcHEP 3.4 for collider physics within and beyond the Standard Model*, Comput.Phys.Commun. **184** (2013) 1729–1769, `arXiv:1207.6082 [hep-ph]`.

[37] J. Alwall, M. Herquet, F. Maltoni, O. Mattelaer, and T. Stelzer, *MadGraph 5 : Going Beyond*, J.High Energy Phys. **1106** (2011) 128, `arXiv:1106.0522 [hep-ph]`.

[38] S. Frixione, P. Nason, and C. Oleari, *Matching NLO QCD computations with Parton Shower simulations: the POWHEG method*, J.High Energy Phys. **0711** (2007) 070, `arXiv:0709.2092 [hep-ph]`.

[39] H.-L. Lai, M. Guzzi, J. Huston, Z. Li, P. M. Nadolsky, et al., *New parton distributions for collider physics*, Phys.Rev. **D82** (2010) 074024, `arXiv:1007.2241 [hep-ph]`.

[40] S. Frixione and B. R. Webber, *Matching NLO QCD computations and parton shower simulations*, J.High Energy Phys. **0206** (2002) 029, `arXiv:hep-ph/0204244 [hep-ph]`.

[41] B. P. Kersevan and E. Richter-Was, *The Monte Carlo event generator AcerMC versions 2.0 to 3.8 with interfaces to PYTHIA 6.4, HERWIG 6.5 and ARIADNE 4.1*, Comput.Phys.Commun. **184** (2013) 919–985, `arXiv:hep-ph/0405247 [hep-ph]`.

[42] G. Corcella, I. Knowles, G. Marchesini, S. Moretti, K. Odagiri, et al., *HERWIG 6: An Event generator for hadron emission reactions with interfering gluons (including supersymmetric processes)*, J.High Energy Phys. **0101** (2001) 010, `arXiv:hep-ph/0011363 [hep-ph]`.

[43] J. M. Butterworth and M. H. Seymour, *Multi-parton interactions in Herwig for the LHC*, http://projects.hepforge.org/jimmy (2007).

[44] T. Gleisberg, S. Hoeche, F. Krauss, M. Schonherr, S. Schumann, et al., *Event generation with SHERPA 1.1*, J.High Energy Phys. **0902** (2009) 007, `arXiv:0811.4622 [hep-ph]`.

[45] P. Golonka and Z. Was, *PHOTOS Monte Carlo: A Precision tool for QED corrections in Z and W decays*, Eur. Phys. J. C **45** (2006) 97, `arXiv:hep-ph/0506026 [hep-ph]`.

[46] ATLAS Collaboration, *ATLAS Simulation Infrastructure*, Eur. Phys. J. C **70** (2010) 823, `arXiv:physics.ins-det/1005.4568 [physics.ins-det]`.

[47] S. Agostinelli et al., *GEANT4: A Simulation toolkit*, Nucl. Instr. Meth. **A506** (2003) 250.

[48] ATLAS Collaboration, *ATLAS tunes of PYTHIA 6 and Pythia 8 for MC11*, ATLAS-PHYS-PUB-2011-009, `https://cds.cern.ch/record/1363300`.

[49] R. Hamberg, W. L. van Neerven, and T. Matsuura, *A Complete calculation of the order α_s^2 correction to the Drell-Yan K factor*, Nucl. Phys. B **359** (1991) 343–405; Erratum–ibid. 644 (2002) 403.

[50] C. Anastasiou, L. Dixon, K. Melnikov, and F. Petriello, *High-precision QCD at hadron colliders: Electroweak gauge boson rapidity distributions at next-to-next-to leading order*, Phys. Rev. D **69** (2004) 094008, `arXiv:hep-ph/0312266 [hep-ph]`.

[51] K. Melnikov and F. Petriello, *Electroweak gauge boson production at hadron colliders through $O(\alpha_s^2)$*, Phys. Rev. D **74** (2006) 114017, `arXiv:hep-ph/0609070 [hep-ph]`.

[52] R. Gavin, Y. Li, F. Petriello, and S. Quackenbush, *FEWZ 2.0: A code for hadronic Z production at next-to-next-to-leading order*, Comput. Phys. Commun. **182** (2011) 2388, `arXiv:1011.3540 [hep-ph]`.

[53] S. G. Bondarenko and A. A. Sapronov, *NLO EW and QCD proton-proton cross section calculations with mcsanc-v1.01*, Comput.Phys.Commun. **184** (2013) 2343–2350, `arXiv:1301.3687 [hep-ph]`.

[54] M. Cacciari, M. Czakon, M. Mangano, A. Mitov, and P. Nason, *Top-pair production at hadron colliders with next-to-next-to-leading logarithmic soft-gluon resummation*, Phys.Lett. **B710** (2012) 612–622, `arXiv:1111.5869 [hep-ph]`.

[55] P. Baernreuther, M. Czakon, and A. Mitov, *Percent Level Precision Physics at the Tevatron: First Genuine NNLO QCD Corrections to $q\bar{q} \to t\bar{t} + X$*, Phys.Rev.Lett. **109** (2012) 132001, `arXiv:1204.5201 [hep-ph]`.

[56] M. Czakon and A. Mitov, *NNLO corrections to top-pair production at hadron colliders: the all-fermionic scattering channels*, J.High Energy Phys. **1212** (2012) 054, `arXiv:1207.0236 [hep-ph]`.

[57] M. Czakon and A. Mitov, *NNLO corrections to top pair production at hadron colliders: the quark-gluon reaction*, J.High Energy Phys. **1301** (2013) 080, `arXiv:1210.6832 [hep-ph]`.

[58] M. Czakon, P. Fiedler, and A. Mitov, *Total Top-Quark Pair-Production Cross Section at Hadron Colliders Through $O(\alpha_S^4)$*, Phys.Rev.Lett. **110** no. 25, (2013) 252004, `arXiv:1303.6254 [hep-ph]`.

[59] M. Czakon and A. Mitov, *Top++: A Program for the Calculation of the Top-Pair Cross-Section at Hadron Colliders*, `arXiv:1112.5675 [hep-ph]`.

[60] R. D. Ball, V. Bertone, S. Carrazza, C. S. Deans, L. Del Debbio, et al., *Parton distributions with LHC data*, Nucl.Phys. **B867** (2013) 244–289, `arXiv:1207.1303 [hep-ph]`.

[61] S. Alekhin, J. Blumlein, and S. Moch, *Parton Distribution Functions and Benchmark Cross Sections at NNLO*, Phys.Rev. **D86** (2012) 054009, `arXiv:1202.2281 [hep-ph]`.

[62] V. Radescu for the H1, ZEUS Collaborations, *Hera Precision Measurements and Impact for LHC Predictions*, `arXiv:1107.4193 [hep-ex]`. HERAPDF 1.5 NLO and NNLO preliminary, H1prelim-11-042, ZEUS-prel-11-002, Proceedings of Moriond 2011.

[63] S. Alekhin, S. Alioli, R. D. Ball, V. Bertone, J. Blumlein, et al., *The PDF4LHC Working Group Interim Report*, arXiv:1101.0536 [hep-ph].

[64] J. Wenninger, *Energy Calibration of the LHC Beams at 4 TeV*, Tech. Rep. CERN-ATS-2013-040, CERN, Geneva, May, 2013.

[65] ATLAS Collaboration, *Selection of jets produced in proton-proton collisions with the ATLAS detector using 2011 data*, ATLAS-CONF-2012-020. http://cdsweb.cern.ch/record/1430034.

[66] ATLAS Collaboration, *Measurement of the top quark-pair production cross section with ATLAS in pp collisions at $\sqrt{s} = 7$ TeV*, Eur. Phys. J. C **71** (2011) 1577, arXiv:1012.1792 [hep-ex].

[67] CMS Collaboration, *Search for new physics in the final states with a lepton and missing transverse energy at $\sqrt{s} = 8$* TeV, CMS Physics Analysis Summary CMS-PAS-EXO-12-060 (2013).